The Plant Cell, Vol. 29: 1184–1195, June 2017, www.plantcell.org © 2017 ASPB.

BREAKTHROUGH REPORT

The RxLR Motif of the Host Targeting Effector AVR3a of *Phytophthora infestans* Is Cleaved before Secretion[OPEN]

Stephan Wawra,[a,1,2] Franziska Trusch,[a,1] Anja Matena,[b] Kostis Apostolakis,[a] Uwe Linne,[c] Igor Zhukov,[d,e] Jan Stanek,[f] Wiktor Koźmiński,[f] Ian Davidson,[g] Chris J. Secombes,[h] Peter Bayer,[b] and Pieter van West[a,3]

[a] Aberdeen Oomycete Laboratory, Institute of Medical Sciences, University of Aberdeen, Foresterhill, Aberdeen AB25 2ZD, United Kingdom
[b] Structural and Medicinal Biochemistry, Centre of Medicinal Biotechnology, University of Duisburg-Essen, 45141 Essen, Germany
[c] Core Facility for Mass Spectrometry and Chemistry, Philipps-Universität Marburg, D-35032 Marburg, Germany
[d] Institute of Biochemistry and Biophysics, Polish Academy of Sciences, 02-106 Warsaw, Poland
[e] NanoBioMedical Centre, Adam Mickiewicz University, 61-614 Poznań, Poland
[f] Biological and Chemical Research Centre (CENT III), Faculty of Chemistry, University of Warsaw, 02-089 Warsaw, Poland
[g] Proteomics Facility, Institute of Medical Sciences, University of Aberdeen, Foresterhill, Aberdeen AB25 2ZD, United Kingdom
[h] Scottish Fish Immunology Research Centre, Institute of Biological and Environmental Sciences, University of Aberdeen, Aberdeen AB24 2TZ, United Kingdom

ORCID IDs: 0000-0003-0608-202X (F.T.); 0000-0002-9912-1018 (I.Z.); 0000-0003-1660-168X (J.S.); 0000-0003-2319-4525 (W.K.); 0000-0001-8781-176X (C.J.S.); 0000-0003-0435-7202 (P.B.); 0000-0002-0767-6017 (P.v.W.)

When plant-pathogenic oomycetes infect their hosts, they employ a large arsenal of effector proteins to establish a successful infection. Some effector proteins are secreted and are destined to be translocated and function inside host cells. The largest group of translocated proteins from oomycetes is the RxLR effectors, defined by their conserved N-terminal Arg-Xaa-Leu-Arg (RxLR) motif. However, the precise role of this motif in the host cell translocation process is unclear. Here, detailed biochemical studies of the RxLR effector AVR3a from the potato pathogen *Phytophthora infestans* are presented. Mass spectrometric analysis revealed that the RxLR sequence of native AVR3a is cleaved off prior to secretion by the pathogen and the N terminus of the mature effector was found likely to be acetylated. High-resolution NMR structure analysis of AVR3a indicates that the RxLR motif is well accessible to potential processing enzymes. Processing and modification of AVR3a is to some extent similar to events occurring with the export element (PEXEL) found in malaria effector proteins from *Plasmodium falciparum*. These findings imply a role for the RxLR motif in the secretion of AVR3a by the pathogen, rather than a direct role in the host cell entry process itself.

INTRODUCTION

Many eukaryotic pathogens including plant pathogenic fungi and oomycetes use effector proteins to successfully infect their hosts. Effectors are secreted molecules that help both the invasion and the propagation of the pathogen by suppressing host defense responses as well as adapting host metabolism (Wawra et al., 2012a).

The phylogenetically related malaria parasites (*Plasmodium* spp) and the plant pathogenic water molds (oomycetes) have numerous effector proteins, which are characterized by conserved N-terminal amino acid sequences (Hiller et al., 2004; Marti et al., 2004) that play a role in the host cell targeting process (Whisson et al., 2007; Boddey et al., 2009). In malaria parasites, the *Plasmodium* export element (PEXEL) consists of Arg-Xaa-Leu-Xaa-Glu/Asp/Gln (with Xaa being any amino acid) positioned close after the signal peptide cleavage site (Hiller et al., 2004; Marti et al., 2004). This sequence element is cleaved by endoplasmic reticulum-located proteases and the N terminus becomes acetylated (Ac-Xaa-Glu/Asp/Gln) (Chang et al., 2008; Boddey et al., 2009, 2010; Russo et al., 2010). The conserved spatial position of the PEXEL motif and its very rapid proteolytic modification are necessary for the export of effector proteins and seem to work as an internal signal for a specialized effector export pathway (Marti and Spielmann, 2013; Boddey et al., 2016). Recently, a similar motif (TEXEL) was found in effector proteins of *Toxoplasma gondii* and reported to play a crucial role in effector maturation and sorting during the infection process (Hammoudi et al., 2015; Coffey et al., 2015; Curt-Varesano et al., 2016).

Numerous effector proteins from plant pathogenic oomycetes carry a similar highly conserved motif: the Arg-Xaa-Leu-Arg (RxLR) motif. This sequence is located within ~40 residues downstream of the secretion signal cleavage site and is often

[1] These authors contributed equally to this work.
[2] Current address: Botanical Institute, Genetical Institute, University of Cologne; Zulpicher Strasse 47a, 50674 Cologne, Germany.
[3] Address correspondence to p.vanwest@abdn.ac.uk.
The author responsible for distribution of materials integral to the findings presented in this article in accordance with the policy described in the Instructions for Authors (www.plantcell.org) is: Pieter van West (p.vanwest@abdn.ac.uk).
[OPEN] Articles can be viewed without a subscription.
www.plantcell.org/cgi/doi/10.1105/tpc.16.00552

followed by another second conserved motif Ser/Asp-Glu-Glu-Arg (s/dEER; reviewed in Wawra et al., 2012a). Effector secretion, and presumably entry into the host cell, happens at the haustorium, an infection-specific interface between pathogen and host that forms after the pathogen has colonized the host (Whisson et al., 2007; Rafiqi et al., 2010). Haustoria are always surrounded by a host plant-derived membrane (Lu et al., 2012). Evidence exists that RxLR effectors translocate after secretion from the extrahaustorial space into plant cells (Whisson et al., 2007; van Poppel et al., 2008; Lokossou et al., 2010; Chou et al., 2011; Gilroy et al., 2011; Saunders et al., 2012). RxLR and RxLR-like effectors may also be present in fungi (summarized in Kale and Tyler, 2011), and different models for the translocation process have been proposed, but the precise mechanism is unclear (Petre and Kamoun, 2014).

Some reports suggest that the RxLR sequences are directly involved in host cell entry. For the RxLR effector avirulence protein 3a (AVR3a) from the potato blight pathogen *Phytophthora infestans*, it was shown that the RxLR motif is required for host cell translocation based on a loss-of-function infection assay (Whisson et al., 2007). In addition, oomycete and fungal RxLR and RxLR-like effectors have been reported to translocate into host cells in the absence of the pathogen (Plett et al., 2011; Gu et al., 2011; summarized in Kale and Tyler, 2011). The autonomous translocation was proposed to occur after binding of the RxLR motif to lipids via phospholipid-mediated endocytosis (Kale et al., 2010). However, this was not observed uniformly for all RxLR effectors and excludes phospholipid binding as a general host entry mechanism (Gan et al., 2010; Yaeno et al., 2011; Wawra et al., 2012b). Furthermore, a recent study indicates that cell-based reentry assays do not support models of pathogen-independent translocation of effectors into plant cells and detected cytosolic amounts of proteins are presumably based on accumulation due to the overexpression of effector proteins (Petre at al., 2016; Na et al., 2013).

The oomycete RxLR motif might have a function similar to the PEXEL motif as a potential internal sorting signal. A fusion protein containing the effector core domain of AVR3a from *P. infestans* coupled to the PEXEL sequence of HRPII (histidine rich protein II) from *Plasmodium falciparum* is delivered into the plant by *P. infestans* (Grouffaud et al., 2008). The equivalent experiment in *Plasmodium*, the delivery of HRPII with the RxLR leader of AVR3a, was also reported to be successful (Bhattacharjee et al., 2006), although this observation was not reproducible in a recent study (Boddey et al., 2016). Nevertheless, RxLR motifs reside within flexible protein regions (Yaeno et al., 2011; Wawra et al., 2012b; Sun et al., 2013) and could be easily accessed by endopeptidases and modified by acetyltransferases. In addition, *P. infestans* also possesses a putative protease similar to the protease responsible for the PEXEL cleavage in *Plasmodium* (Boddey et al., 2010; Kay et al., 2011).

Here, we investigated the biochemical integrity of the native RxLR effector AVR3a secreted into culture filtrate of axenically grown *P. infestans.* In combination with the structural analysis of recombinant AVR3a by NMR spectroscopy, the obtained data support a model comprising the processing of the effector RxLR sequence before secretion.

RESULTS

To investigate the potential processing of the RxLR motif of RxLR effector proteins from *P. infestans*, ideally the proteins should be obtained from the interhaustorial space of infected plant material. However, as the quantities of effector produced during infection are negligible it is not feasible with the current available technology to isolate and purify suitable amounts of secreted effectors for biophysical studies. Therefore, an RxLR effector protein from culture filtrate was purified. The only validated effector candidate that is secreted in reasonable quantities into the culture filtrate of *P. infestans* is the RxLR effector AVR3a (Torto et al., 2003). Since tagging and/or modification of the sequence can impair the biophysical properties of the effector (Wawra et al., 2012b), we focused on native AVR3a secreted during axenic growth of in vitro-cultivated *P. infestans*. The enrichment of the naturally occurring variant AVR3a^{EM} [AVR3a(S19)E80M103] from the supernatant of an axenic culture was optimized and native AVR3a was purified (Figure 1A). The corresponding bands on SDS-PAGE were analyzed by liquid chromatography-tandem mass spectrometry (LC-MS/MS), and AVR3a^{EM} (gi|289470504) was identified through the detection of several peptides with significant thresholds using two different mass spectrometers (Figure 1B). Interestingly, no peptides were detected N-terminally of the RxLR motif, but a "KNEENEETSEER" peptide starting immediately after the RxLR motif was identified (Figure 1C; ion score, 54; e-value, 3.8e-01). The weak MS/MS fragmentation of the "KNEENEETSEER" peptide is likely caused by the acidic character (6 $\times$ Glu), which results in elution very early in the LC run and insufficient ionization for mass spectrometry. A control spectrum of a 10-fold amount of recombinant AVR3a$_{22\text{-}147}$ protein containing the residues N-terminal to the RxLR motif resulted in a similar weak spectrum for the same peptide (ion score, 21; e-value, 1.8e-01). The mass spectrometric data also support the prediction of the N-terminal acetylation of native AVR3a (e-value, 1.7e+02), which would be possible only if the RxLR is cleaved before secretion of AVR3a, rendering the N terminus of the corresponding lysine accessible to acetyltransferases, which are exclusively intracellular.

To further test for the potential cleavage of the RxLR motif in AVR3a, native AVR3a was separated by reverse-phase (RP) chromatography and the main constituent of the sample was subsequently analyzed by MALDI-TOF to determine its absolute molecular mass (Figure 1D). Several peaks were observed, but most interestingly in the mass range of 11.5 to 13 kD, peaks showed a Gaussian distribution with a separation of Δ162 D. This pattern is typical for protein glycosylation (Mirgorodskaya et al., 2000); therefore, the remaining fraction was lyophilized and enzymatically deglycosylated. Trichloroacetic acid (TCA) precipitation and subsequent SDS-PAGE analysis revealed a band shift for AVR3a corresponding to a lower molecular mass; such a shift was not observed for recombinant AVR3a$_{48\text{-}147}$ (Figure 1E). The shifted band was analyzed via LC-MS/MS and also identified as AVR3a^{EM} through the detection of the same peptides as for the glycosylated form (Figure 1B). In addition, the band corresponding to the deglycosylated AVR3a was reanalyzed by MALDI-TOF and instead of the Gaussian distributed peak group, this time only one peak for AVR3a was detected. The exact molecular mass of 11,621 D was confirmed after internal calibration with cytochrome

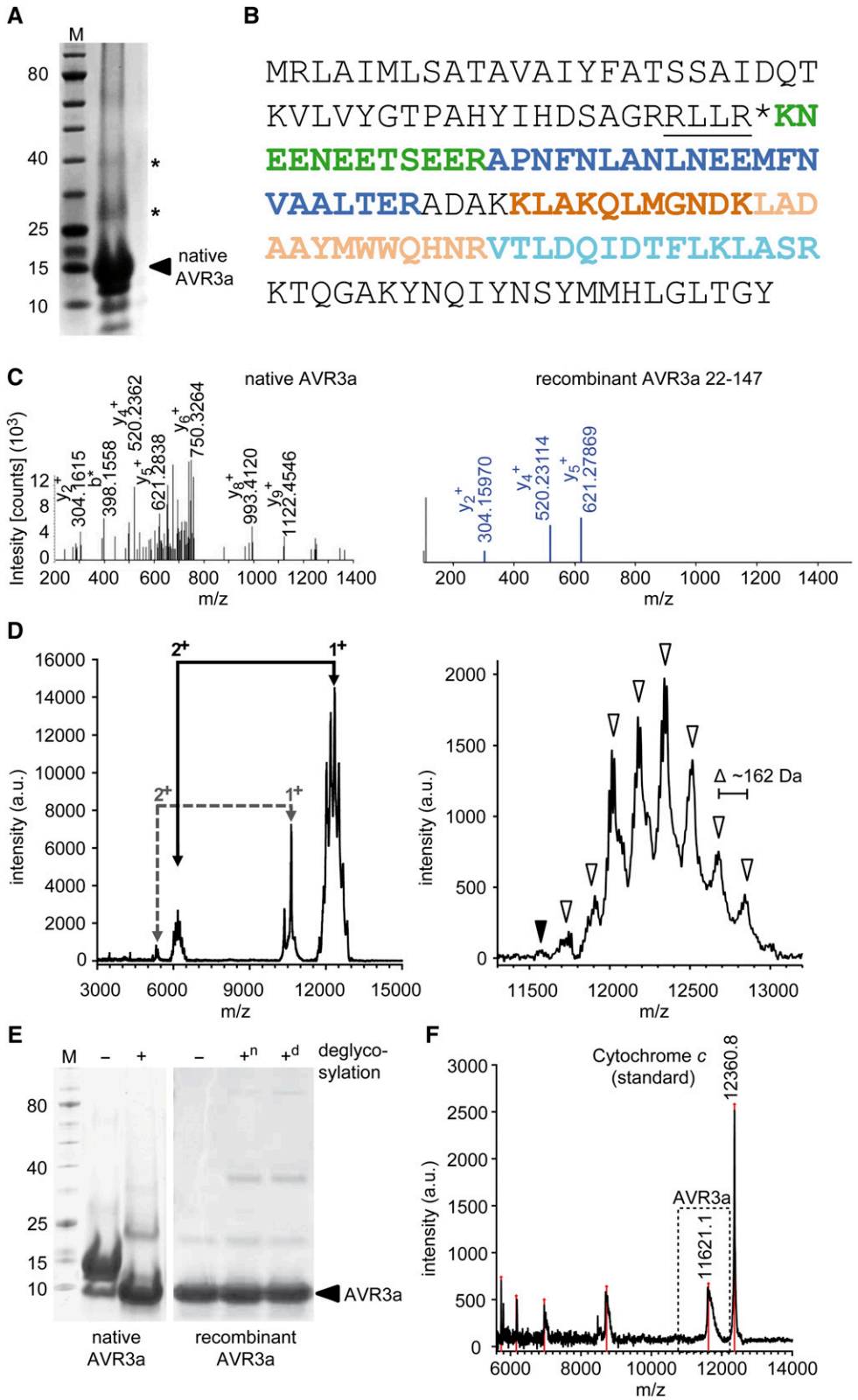

Figure 1. Purification of Native Processed AVR3a from *P. infestans* Culture Filtrate and MALDI-TOF Analysis.

(A) SDS-PAGE of native AVR3a purified from axenic growth culture of *P. infestans*. All bands on the gel were identified by LC-MS/MS as AVR3aEM, which seems to form SDS-resistant multimers (asterisks).

(B) Amino acid sequence of AVR3aEM from *P. infestans* isolate 88069. Peptides are highlighted according to their detection by LC-MS/MS (green), nanoRSLC-HPLC (orange), or both methods (blue). The RxLR motif is underlined, and the cleavage site is highlighted by an asterisk.

c (Figure 1F). The occurrence of a single peak indicates that there was complete deglycosylation of the up to nine hexose units in native AVR3a and thereby excluded the presence of multiple cleaved polypeptides. The closest mass match of AVR3a to the measured 11,621 D is a polypeptide including amino acids 48 to 147 (11,577 D), especially considering that processing from the C terminus is unlikely due to the physiological importance of Tyr147 of AVR3a (Bos et al., 2010).

However, the observed +44 D difference between the theoretical mass and the experimentally determined mass of AVR3a$_{48-147}$ is too large to be considered an error. Indeed, a polypeptide mass difference of +44 D would correspond exactly to an acetyl modification (with an additional H^+) of AVR3a$_{48-147}$, which is in perfect agreement with the data obtained from the initial LC-MS/MS analysis (Figure 1B). To validate the LC-MS/MS data that indicated an *N*-acetylation at amino acid 48 (RLLR*K), Edman degradation was performed. Edman degradation results in chemical cleavage of the N-terminal peptide bond of a polypeptide chain only when the amino group is sterically accessible and not modified in any way (Edman, 1950). To reduce potential side reactions, Edman degradation was performed with deglycosylated AVR3a and, indeed, no significant amino acid sequence could be detected despite employing a sufficient quantity of AVR3a (data not shown). Consequently, the experimentally obtained mass difference of +44 D between the measured and the theoretical expected mass for AVR3a$_{48-147}$ and the N-terminal blockage observed by Edman sequencing indicates that native AVR3a secreted by an axenic *P. infestans* culture into the medium is cleaved at R47 after the RxLR motif and probably is *N*-acetylated at Lys-48, the first amino acid downstream of the RxLR.

Since Kay et al. (2011) described a phylogenetic homology between the PEXEL-cleaving plasmepsin V from *P. falciparum* and PiAP12 of *P. infestans*, we overexpressed the protease domain of PiAP12 (79–432 amino acids) in *Escherichia coli* and purified the soluble fraction (Figure 2A, left). We incubated the PiAP12-containing fractions with 5 μg AVR3a$_{22-147}$ for 1 h at 37°C. However, no differences in the band patterns were observed compared with the control, even after reduction of the pH (Figure 2A, right). Since impurities might disturb the activity of the protease, we performed another purification of the elution fractions under denaturing conditions. After refolding, PiAP12 remained unable to process recombinant AVR3a (Figure 2B). Hence, we cloned the other 10 aspartic proteases of *P. infestans*. To avoid any precipitation and inactivation of the proteases during the purification procedure, we cotransformed the catalytic domain of each protease with AVR3a$_{22-147}$ into *E. coli*. We reasoned that the simultaneous expression of both proteins should increase our chances of detecting any potential proteolytic activity. Although each of the aspartic protease domains could be detected in the soluble fraction without significant degradation, no additional bands for AVR3a$_{22-147}$ could be observed, indicating a lack of cleavage (Figure 2C).

Another interesting biochemical feature of native AVR3a^{EM} seems to be the formation of stable multimers that can be observed after SDS-PAGE (asterisks in Figure 1A). To explore this multimer formation further, ^{15}N-labeled AVR3a$_{48-147}$ was overexpressed (Figure 3A), the backbone atoms assigned, and the relaxation times measured by NMR spectroscopy. From the relaxation times, we estimated the rotation correlation time (τ_c), which correlates to the size of the protein (Figure 3B). The T_1/T_2 constant ratio was 30.5 ± 2.7 ms and equal to a molecular mass of 24 kD, confirming the dimerization of recombinant AVR3a$_{48-147}$. By contrast, AVR3a$_{60-147}$ was shown to behave like a monomer (Wawra et al., 2012b), which is in line with our relaxation data (T_1/T_2 = 6.9 ± 0.3 ms) and an estimated molecular mass of 11 kD.

For a detailed understanding of the dimerization interface, several 2D-, 3D-, and 4D-NMR spectra of AVR3a$_{60-147}$ were measured, and the backbone as well as side chain atoms assigned because the monomeric state is more suitable for NMR studies. The NMR solution structure of AVR3a$_{60-147}$ adopted the typical 4 α-helix bundle in the core domain with a flexible, disordered N terminus until Glu-70 (Figure 3C, Table 1) that was also observed for the *Phytophthora capsici* homolog AVR3a4 (Yaeno et al., 2011). The alignment of the AVR3a$_{60-147}$ structure with the structures of AVR3a4 and AVR3a11 from *P. capsici* showed high similarity, with RMSD values of 3.1 and 3.3 Å, respectively (Figure 3D). Furthermore, the electrostatic potential of the molecular surface of AVR3a$_{60-147}$ was calculated with Pymol using the Poisson Boltzmann Equation (Baker et al., 2001). As already speculated from homology models of AVR3a$_{60-147}$, a positively charged patch on the surface of the core domain was formed by Lys-85, Lys-86, Lys-89, Arg-124, Lys-125, and Lys-130 (Figure 3E). The formation of a positively charged patch seems to be restricted to AVR3a-like effectors since no patches could be found in effector proteins like PexRD2 or ATR1 although their folds are highly similar (data not shown; Win et al., 2012).

Based on our above results, we concluded that (1) AVR3a$_{60-147}$ is a monomer, while AVR3a$_{48-147}$ forms a homodimer, and (2) residues 48 to 59 (KNEENEETSEER) are essential for the multimerization of native as well as recombinant AVR3a as already

Figure 1. (continued).

(C) MS/MS fragmentation of the peptide KNEENEESTEER of native AVR3a originating from the main band in **(A)** (left; HCT ultra PTM Discovery System; Bruker) and recombinant AVR3a22-147 6x His-tag (right; Q Exactive Hybrid Quadrupole-Orbitrap; Bruker).

(D) Left: MALDI-TOF spectrum of native AVR3a (main constitution from reverse-phase liquid chromatography), recorded with a 2,5-dihydroxybenzoic acid matrix. Right: Detail of spectrum of native AVR3a (mass area: 11.4–13.2 kD), recorded with a α-cyano-4-hydroxycinnamic acid matrix. Arrowheads highlight peaks with a mass difference of ~162 D.

(E) SDS-PAGE of purified native AVR3a (left) and recombinant AVR3a48-147 (right) before and after incubation with an enzymatic deglycosylation mix. Additional bands originate from the enzyme mix. n, native conditions; d, denaturing conditions.

(F) A molecular mass for AVR3aEM of 11,621 D was obtained after deglycosylation (square) and internal calibration with cytochrome *c*. The same mass was also found to a lesser extent in the untreated sample (filled arrowhead in **[D]**).

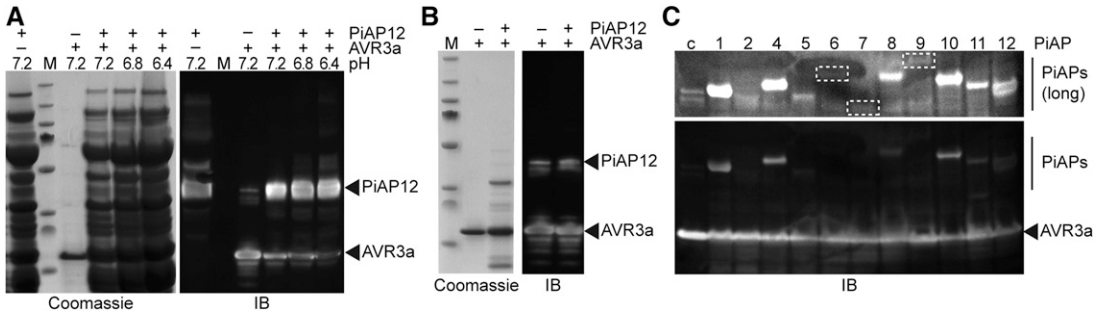

Figure 2. Recombinant AVR3a22-147 Is Not Cleaved by Catalytic Domains of Aspartic Proteases in Vitro.

(A) SDS-PAGE and immunoblot of the elution fraction containing the PiAP12 domain and coincubation with recombinant AVR3a22-147 containing the N-terminal RxLR sequence for 1 h at 37°C at pH values as indicated. No additional bands for AVR3a appeared.

(B) SDS-PAGE and immunoblot of the elution fraction with refolded PiAP12 after purification under denaturing conditions and coincubation with recombinant AVR3a22-147 for 1 h at 37°C. Again, no additional bands for AVR3a were observed.

(C) Soluble fractions of *Escherichia coli* coexpressing AVR3a22-147 6xHis and each protease domain as indicated (c, recombinant AVR3a22-147 6× His; dashed boxes indicate bands less soluble proteases; upper blot is with extended exposure time). No additional bands of AVR3a were observed under these conditions that indicate proteolytic activity of the protease domains.

postulated by Wawra et al. (2012b). To evaluate the influence of the positively charged poly-E linker on the multimerization of AVR3a, the charge of the N terminus (K48-R59) was changed by mutating all six glutamates to glutamines. In line with the hypothesis of an electrostatic-mediated dimerization, the mutant was monomeric according to the time constant ratio of 10.1 ± 0.6 ms, which indicated a mass of 13 kD similar to that of $AVR3a_{60-147}$ (Figure 3B). The tendency for the multimerization of wild-type $AVR3a_{48-147}$ in contrast to the monomeric state of the poly-E/Q mutant was also observed by size-exclusion chromatography (SEC) (Figure 3F). Although the flexible N terminus of AVR3a caused a bigger hydrodynamic radius that leads to shorter running times in SEC experiments, the appearance of one peak for the mutant and two peaks for the wild type clearly pointed toward a multimerization phenomenon mediated by the poly-E stretch.

DISCUSSION

This study shows that native $AVR3a^{EM}$ is cleaved and probably *N*-acetylated downstream of the RxLR motif by *P. infestans* before secretion into culture filtrate and that it forms stable multimers. *N*-acetylation is mediated by N-terminal acetyltransferases. Since N-terminal acetyltransferases are exclusively intracellular enzymes, *N*-acetylation of proteins after secretion is not possible (Starheim et al., 2012). Hence, the intracellular cleavage of AVR3a is a prerequisite for the potential acetylation of the N-terminal Lys-48 and cleavage by proteases of *P. infestans* cosecreted into the culture filtrate can be excluded.

The cleavage site directly after the RxLR sequence and the high conservation among other effector proteins suggest that the RxLR motif might play a crucial role in the intracellular processing before secretion. Notably, the RxLR effector Avh241 from *Phytophthora sojae* contains a myristoylation motif (GAAKAK) after its RxLR motif (Yu et al., 2012). In general, myristoylation sites are located at the N terminus of a protein. Based on our model invoking RxLR processing, this myristoylation modification site in Avh241 would no longer lie within the sequence but instead would be present at the very N terminus after removal of the RxLR motif (RWLR).

We have not directly shown that processed AVR3a is able to translocate into plant cells; thus, we cannot completely rule out that an alternative pathway might be involved during infection. However, the model whereby the RxLR motif is involved in secretion rather than working as an uptake motif is strongly supported by the fact that an RxLR deletion construct of AVR3a still showed translocation activity (Kemen et al., 2011). Based on our study, mutations or deletions of RxLR leaders could result not only in miscleavage and concomitant missorting, but also possibly protein destabilization. Hence, loss-of-function phenotypes can even occur when the effector translocation process is not impaired. Accordingly, the loss-of-recognition phenotype of *P. infestans*-delivered AVR3a mutants (Whisson et al., 2007) or *P. sojae*-delivered AVR1b mutants (Dou et al., 2008) could be caused by defects of effector sorting and/or stabilization. Furthermore, results of studies in which chimeric proteins containing the effector domain of AVR3a and N-terminal sequences of other effectors, especially in model systems without the natural host-pathogen interaction, should be revisited (Anderson et al., 2012; Stassen et al., 2013). Negative results might be due to the lack of the correct processing of the N terminus and concomitant secretion and ultimately not caused by the loss of their translocation abilities into the host.

In general, the current models for pathogen-independent host cell uptake and endocytosis of effector proteins via RxLR binding to plant cell surface phospholipids should probably be revisited (Kale et al., 2010; Ellis and Dodds, 2011; Wawra et al., 2012b). Our study also strengthens the model whereby the lipid binding of effector proteins is mainly mediated by a positively charged lysine patch on the surface of the core domains rather than the RxLR motif in the N terminus (Sun et al., 2013; Yaeno and Shirasu, 2013; Lu et al., 2013). Since the lipid binding and the multimerization are mediated by the same patch, masking of the lysine patch by the N terminus of AVR3a might also have a protective function to avoid unspecific interactions during the translocation process.

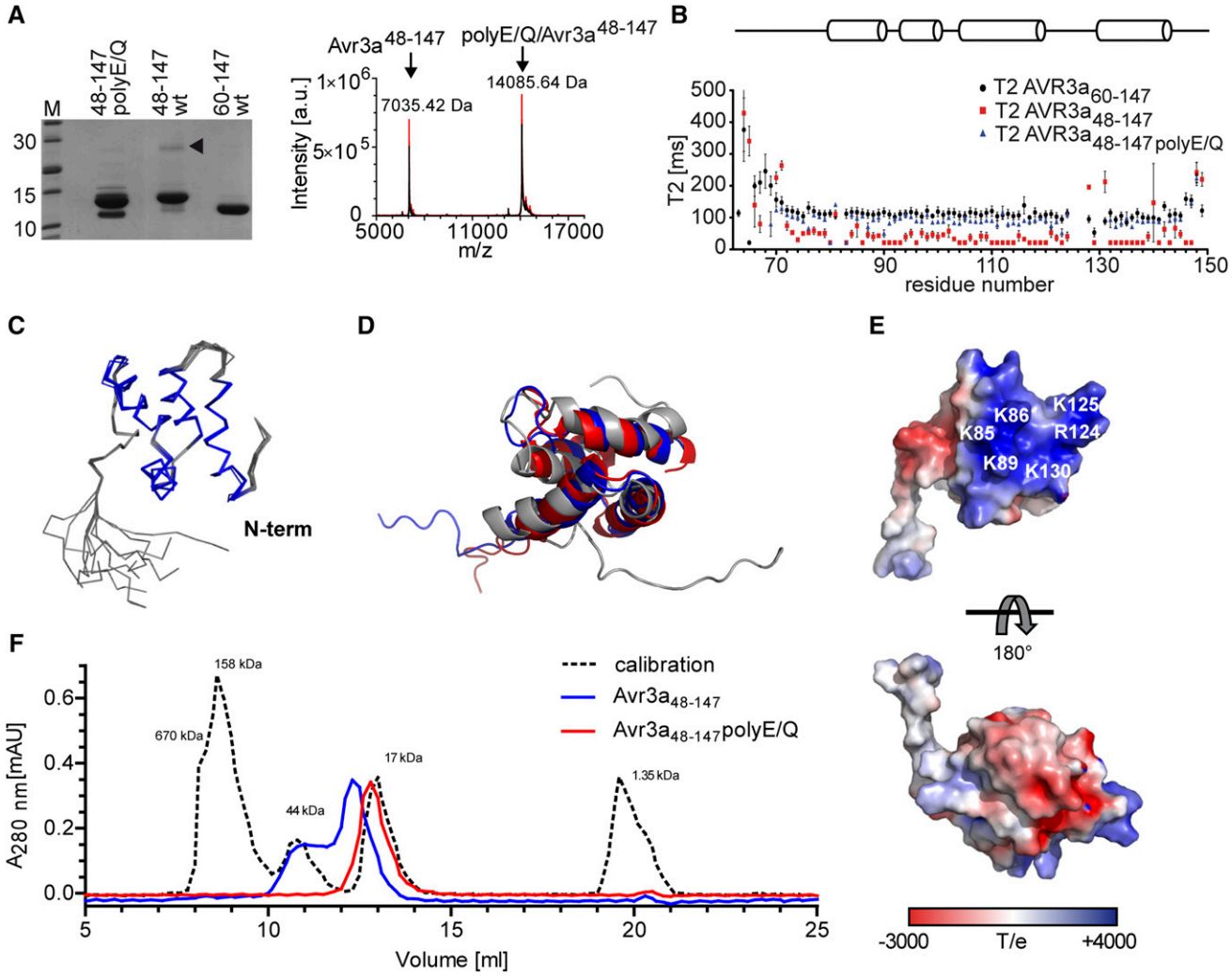

Figure 3. Solution Structure of Recombinant AVR3a60-147 and Characterization of the Dimerization Interface.

(A) SDS-PAGE (left) and MALDI-TOF spectra (right) of recombinant 15N-labeled AVR3a constructs used for NMR experiments. The arrowhead indicates SDS-resistant multimers.

(B) T_2 times for different AVR3a constructs for the determination of the molecular mass. The secondary structure of AVR3a60-147 is shown above.

(C) A bundle of the 10 lowest energy structures of recombinantly expressed AVR3a60-147 (without visualization of the C-terminal His-tag). The RxLR effector characteristic 4 α-helix bundle that follows a disordered N terminus is shown in blue.

(D) Overlay of AVR3a60-147 (gray) with the structures of AVR3a4 (blue; PDB-ID: 2LC2) and AVR3a11 (red; PDB-ID: 3ZGK) from *P. capsici* revealed a high structural homology.

(E) Electrostatic surface potential (PBE) of AVR3a60-147 is shown. The positively charged patch on the surface of AVR3a is built up by Lys-85, Lys-86, Lys-89, Arg-124, Lys-125, and Lys-130 as indicated.

(F) SEC of wild-type AVR3a48-147 compared with AVR3a48-147 polyE/Q mutant. For AVR3a48-147 poly-E/Q, only one peak (22 kD) appears in the chromatogram, while the wild type shows two peaks (27 and 50 kD), indicating multimerization for the wild type.

The NMR solution structure of $AVR3a_{60-147}$ reflects mainly the results obtained from an AVR3a4-based homology model (Yaeno et al., 2011). AVR3a comprises a three-helix WY domain with an N-terminal extension that forms a typical four-helix bundle (Win et al., 2012). The rigid core domain contains the amino acids Glu-70 to Tyr-147, while the N terminus is flexible and disordered and not incorporated into the core structure that is an essential prerequisite for the cleavage by a protease. Notably, the N terminus (Lys48-Arg59) of $AVR3a_{48-147}$ is also involved in the dimerization, as demonstrated by earlier cross-linking studies (Wawra et al., 2012b). Our results suggest that an initially weak multimerization of the AVR3a core domain is highly stabilized by the electrostatic interaction between the negatively charged N terminus containing the poly-E stretch and the positively charged patch at the surface of the core domain (Figure 3). The poly-E-mediated multimerization of AVR3a likely does not influence the lipid binding

Table 1. Statistics for the Solution Structure Calculation of AVR3a$_{60-147}$

Number of distance and dihedral angle constraints	
Total NOEs	1287
Intraresidual NOEs	269
Sequential NOEs (i to i + 1)	351
Medium-range NOEs (i to i + 2,3,4)	311
Long-range NOEs	356
Dihedral angle restraints ($\varphi + \psi$)	61 + 61
RMSD to the mean structure (Å)	
RMSD for backbone atoms (T80-G144)	0.30 ± 0.09
RMSD for heavy chain atoms (T80-G144)	0.98 ± 0.17
Average target function	1.39 ± 0.07
Restraint violations	
Average of upper distance (Å)	0.006 ± 0.001
Average of maximum upper distance (Å)	0.22 ± 0.07
Average of sum of van der Waals (Å)	6.2 ± 0.2
Average of torsion angle (°)	0.464 ± 0.034
Average of maximum torsion angle (°)	2.43 ± 0.35
Ramachandran analysis (%)	
Residues in most favored regions	75.2
Residues in additionally allowed regions	24.6
Residues in the generously allowed regions	0.0
Residues in the disallowed regions	0.2

Data are derived from a set of the 10 lowest-energy structures calculated by CYANA 2.1 using automated NOE (nuclear Overhauser effect) assignment without a homology model. RMSD, root mean square deviation.

properties of AVR3a because mutation of the RxLR motif of the effector AVR1d (RxLR/EEEE) does not have an effect on lipid binding (Na et al., 2013). Thus, as mentioned above, the N terminus serves to mask the positively charged patch of the core domain to avoid unspecific interaction during secretion and translocation until the point of membrane-mediated uptake into the host cell. Multimerization of another effector protein, PexRD2, is essential for its function in planta (King et al., 2014). Hence, the dimerization of AVR3a might be essential for its interaction with potato R3a since the different R3a recognition sites (K/E80 and I/M103), which are important for the hypersensitive response in planta, do not interfere with the multimerization (Bos et al., 2006).

The processing of native AVR3a secreted from *P. infestans* is indeed remarkably similar to the cleavage observed for the PEXEL motif of effectors from *P. falciparum* (Chang et al., 2008; Boddey et al., 2009; Russo et al., 2010) (Figure 4) and also for the TEXEL motif of effectors from *T. gondii* (Coffey et al., 2015; Curt-Varesano et al., 2016). However, the RxLR motif is not recognized and cleaved by the ER-located plasmepsin V protease of *P. falciparum* (Boddey et al., 2016). Furthermore, despite the phylogenetic relationship between plasmepsin V from *P. falciparum* and PiAP12 (Kay et al., 2011), we could not detect any proteolytic activity against recombinant AVR3a$_{22-147}$ for PiAP12 nor for any of the other 10 aspartic protease domains (Figure 2C). An analogous system might exist in *P. infestans* with a similar mode of action as in *P. falciparum* but having evolved from a different origin. In contrast to the PEXEL motif, which is partly retained after processing (Ac-X-E/D/Q) (Chang et al., 2008), the RxLR sequence of AVR3a^{EM} is cleaved off completely. The cleaved PEXEL motif is involved in the binding of the respective effector to the PTEX red blood cell import translocon (Boddey et al., 2009; Russo et al., 2010). It is intriguing to speculate what role might be played by the retained s/dEER sequence that is conserved in many RxLR effectors. Although the protein export and host cell translocation mechanisms between the pathogens are not interchangeable, probably due to their

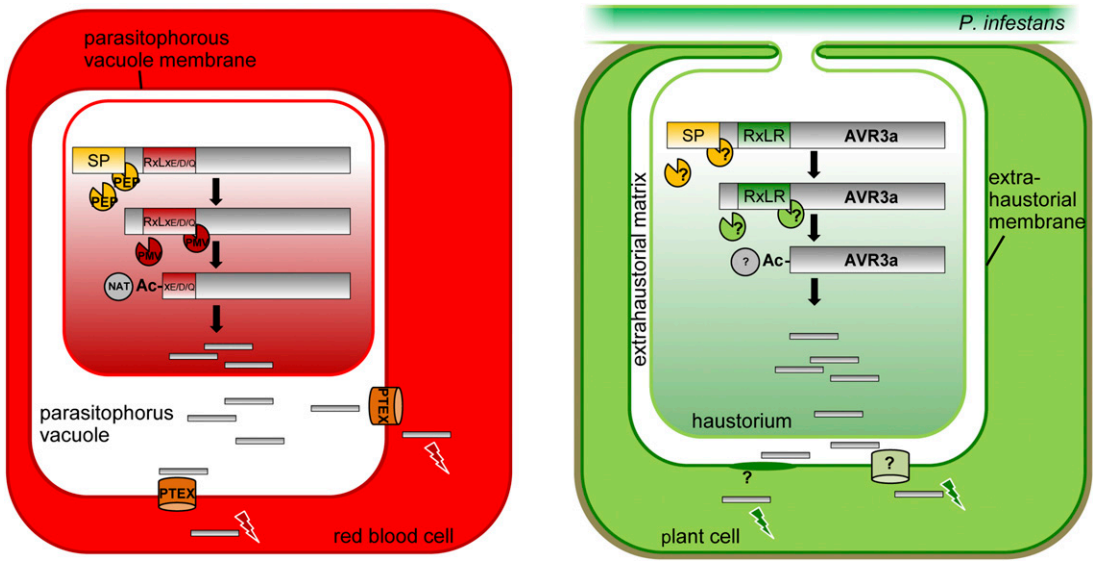

Figure 4. Comparison of the Processing of the PEXEL Motif in *P. falciparum* and the RxLR Motif of AVR3a in *P. infestans*.

The processing of AVR3a is strikingly similar to the stepwise modification observed for the PEXEL effectors from *P. falciparum*. However, the PEXEL motif (RxLxE/D/Q) is partially retained, while the RxLR motif is cleaved off completely, although both are acetylated (Ac). The corresponding RxLR-modifying enzymes remain to be investigated. NAT, N-terminal acetyltransferase; PEP, signal peptide peptidase; PMV, plasmepsin V; PTEX, *Plasmodium* translocon of exported proteins; SP, signal peptide.

different infection structures (intracellular parasitophorous vacuoles for *P. falciparum*/*T. gondii* versus extracellular haustoria for oomycetes), the stepwise processing of the RxLR motif in oomycetes could act as a signal that facilitates the transport to and secretion of effectors from the haustorial infection structure similarly to PEXEL and TEXEL.

METHODS

Purification of Native AVR3a^{EM}

To establish a purification protocol for native AVR3a, initially the optimization was done with *Phytophthora infestans* transformants carrying a translational AVR3a-mRFP fusion protein (AVR3a^{KI}:mRFP) as described previously (Whisson et al., 2007). For the purification of native AVR3a^{EM}, 6 liters of a liquid culture of *P. infestans* (isolate 88069) in pea broth was grown in several Petri dishes (each 75 mL) for 22 d to confluence. Mycelium was removed by paper filtration and the supernatant cleared by centrifugation (15 min, 15,000*g*) and an additional filtration step (0.45 μm, nitrocellulose). The supernatant was supplemented with 2 mM EDTA and a protease inhibitor mix (two tablets/3 liters; Roche). Afterwards, the protein suspension was loaded onto a SO_3^- column (Fractogel-EMD-SO^{3-}; Merck) for initial concentration. The column was washed once with 25 mM NaP_i buffer, pH 7.3, and once more with the same buffer containing 80 mM NaCl. Subsequently, bound proteins were eluted with the same buffer supplemented with 1 M NaCl and the protease inhibitor AEBSF. The elution fraction was ammonium sulfate precipitated (80%) for 30 min at room temperature. Pellets obtained from precipitation after centrifugation (20 min, 9000*g*) were resuspended in 20 mL of 50 mM NaP_i buffer, pH 7.3, and additionally dialyzed (1 × 3 liters for 3 h and 1 × 3 liters overnight) against NaP_i buffer supplemented with 15 mM $MgSO_4$. The dialyzed protein fractions were resubjected to the SO^{3-} column to remove remaining contaminants and washed twice with 25 mM NaP_i buffer, pH 7.3 (the second one with additional 100 mM NaCl), followed by elution with the same buffer supplemented with 200 mM NaCl. An aliquot was TCA precipitated and prominent bands on SDS-PAGE were analyzed by LC-MS/MS. The results in this study arose from several independent preparations of AVR3a from in total 70 liters of *P. infestans* culture.

TCA Precipitation

For 300- to 500-μL sample, 1 mL of 40% TCA was used for protein precipitation overnight at 4°C. Subsequently, samples were centrifuged for 30 min at 16,000*g* (4°C) and the supernatant was discarded. The remaining pellet was washed with 1 mL acetone and centrifuged again for 20 min at 16,000*g* (4°C). This step was repeated twice before drying the pellet.

LC-MS/MS Analysis

Proteins of interest from SDS-PAGE were trypsin digested, dried, and resuspended in 0.1% formic acid. Dissolved peptides were analyzed using an HCT ultra PTM Discovery System with an electrospray source fitted with a low-flow nebulizer (Bruker) coupled to an UltiMate 3000 LC system (Thermo Fisher Scientific). Peptides were separated on a PepSwift monolithic PS-DVB capillary column (200 μm i.d. × 5 cm; Thermo Fisher Scientific) at a flow rate of 2.0 μL/min. Eluent A (3% acetonitrile/0.05% formic acid) and Eluent B (80% acetonitrile/0.04% formic acid) were used for a gradient (3% to 45% B, 12 min), followed by a column wash (90% B, 1 min) and an equilibration step (3% B, 5 min). MS/MS data, averaged from two spectra, with a scan range of 100 to 2200 *m/z*, were acquired in data-dependent AutoMS(2) mode. Up to three precursor ions were selected from the MS scan (range 300 to 1500 *m/z*, averages 3) in each cycle. Singly charged ions and precursors were actively excluded after selection twice within a 1.0-min window. Peptide peaks were detected and deconvoluted automatically using DataAnalysis software (Bruker). Mass lists were created automatically and used as the input for Mascot MS/MS ion searches of the NCBInr database (www.matrixscience.com). The Mascot significance threshold was set to <0.05. Default search parameters were enzyme = trypsin; maximum missed cleavages = 1; fixed modifications = carbamidomethyl (C); variable modifications = oxidation (M); acetyl (N-term) and deamination (NQ); peptide tolerance = ±1.5 D; MS/MS tolerance ± 0.5 D; peptide charge = 2+ and 3+; instrument = ESI-TRAP.

NanoRSLC-HPLC Analysis

Mass spectrometric analysis of the digested peptides was performed using an Orbitrap Velos Pro mass spectrometer (Thermo Scientific). An Ultimate nanoRSLC-HPLC system (Thermo Scientific) equipped with a nano C18 RP column was connected online to the mass spectrometer through a nanospray ion source. The tryptic digest (6 μL) was injected onto a C18 preconcentration column. Automated trapping and desalting of the sample were performed at a flow rate of 6 μL/min with 0.05% formic acid. Eluent A (0.045% formic acid) and Eluent B (80% acetonitrile/0.05% formic acid) were used. Separation was achieved with a gradient (4% to 45% B, 30 min) at a flow rate of 300 nL/min, followed by a column wash (95% B, 5 min). The column was connected to a stainless steel nanoemitter (Thermo Scientific) and the eluent sprayed directly toward the heated capillary of the mass spectrometer using a potential of 2300 V. A survey scan with a resolution of 60,000 within the Orbitrap mass analyzer was combined with at least three data-dependent MS/MS scans with dynamic exclusion for 30 s either using CID with the linear ion trap or using HCD and Orbitrap detection at a resolution of 7500. Data analysis was performed using Proteome Discoverer (Thermo Scientific) with SEQUEST and MASCOT (version 2.2; Matrix Science) search.

Reverse-Phase Liquid Chromatography

TCA precipitated pellets were dissolved in 50 μL of 0.1% trifluoroacetic acid (TFA) and subjected to reverse-phase separation. Reverse-phase liquid chromatography was carried out using an UltiMate3000 system (Thermo Fisher Scientific) equipped with a YMC-Pack Protein-RP column (YMC Europe; 100 × 2.1 mm S-5 μm). Eluent A (0.1% TFA) and Eluent B (80% acetonitrile, 0.085% TFA) were used. The flow rate was set to 100 μL/min with a gradient of 0 to 70% B for 25 min. Fractions of 100 μL were collected.

MALDI-TOF

All spectra were acquired on an ultrafleXtreme MALDI-ToF/ToF mass spectrometer (Bruker) equipped with a 1-kHz Bruker Smartbeam-II solid-state laser. A 2,5-dihydroxybenzoic acid or a α-cyano-4-hydroxycinnamic acid carrier matrix was used as indicated. Linear mode acquisition was performed with a high resolution in a 3000 to 20,000 *m/z* range, and the sample rate was 1.00 GS/s with Bruker Protein Calibration I Standard P/N 206355. Between 1000 and 10,000 shots were accumulated manually with Smartbeam laser focus raster width set at 50 μm. Spectra were processed in Compass 1.3 software incorporating Flex Control version 3.3 and Flex Analysis version 3.3 using "centroid" peak picking (80%), smoothing performed using Savitzky-Golay 0.2 *m/z* for one cycle, and TopHat baseline subtraction for reproducible peak annotation on nonresolved isotope distributions prior to calibration.

Enzymatic Deglycosylation

Enzymatic deglycosylation was performed on either lyophilized samples or protein pellets obtained after TCA precipitation. The denaturing reaction conditions protocol provided with the New England Biolabs Protein

Deglycosylation Mix (P6039S) was chosen. Deglycosylation was carried overnight at 37°C.

Cloning and Mutagenesis

The sequences encoding $AVR3a_{48\text{-}147}$ and $AVR3a_{48\text{-}147}$ poly-E/Q (E50Q, E51Q, E53Q, E54Q, E57Q, and E58Q) were PCR amplified with oligonucleotides as indicated in Supplemental Table 1 using *AVR3a*$_{22\text{-}147}$ as a template (Wawra et al., 2012b). The resulting fragments containing the restriction sites for *Nde*I and *Eco*R1 (NEB) were cloned into a pET21b vector. Constructs were confirmed by Sanger sequencing (OneSource Bioscience).

Sequences encoding the aspartic proteases were PCR amplified with oligonucleotides as indicated in Supplemental Table 1 using cDNA from *P. infestans* (isolate 88069) as a template. The resulting fragments containing the restriction sites for *Nde*I and *Eco*R1 or *Nde*I and *Eco*R1 (NEB) for PiAP were cloned into a pET21b vector. Constructs were confirmed by Sanger sequencing (OneSource Bioscience).

$AVR3a_{22\text{-}147}$ containing the N-terminal RxLR motif was cloned into pHisTEV (kanamycin resistance, C-terminal 6× His-tag) with *Nde*I/*Xho*I using *AVR3a*$_{22\text{-}147}$ as a template (Wawra et al., 2012b). Constructs were confirmed by Sanger sequencing (OneSource Bioscience).

Expression and Purification of Recombinant AVR3a Constructs

Recombinant AVR3a protein containing a C-terminal 6x His-tag was obtained as described elsewhere (Wawra et al., 2012b). Briefly, for isotopically labeled protein, cells from 0.5 liters LB culture (OD_{600} of 0.8) were transferred to 2 liters M9 minimal medium supplemented with 1 g/L [^{15}N] NH_4Cl and/or 0.4% (w/v) [U-^{13}C]glucose and further grown to an OD_{600} of 0.8. Subsequently, protein expression was induced with 0.2 mM IPTG overnight at 25°C. Cells were collected, lysed by sonication (60% intensity, 4 × 45 s, 1 min interval at 4°C; Sonoplus; Bandelin), and ultracentrifuged (Beckman Coulter; 98,000*g*, 70 min, 4°C). Subsequently, the supernatant was applied to a Q-Sepharose column (equilibrated with 50 mM KPi buffer, pH 6.5). The flow-through containing AVR3a was applied to a Ni-NTA column equilibrated with 50 mM KPi buffer, pH 6.5, 500 mM KCl, and 20 mM imidazole. After a washing step, proteins were eluted with 300 mM imidazole. Fractions containing the AVR3a proteins were pooled and the imidazole removed by dialysis for NMR spectroscopy. The integrity of each construct was confirmed by SDS-PAGE and MALDI-TOF mass spectrometry.

Expression and Purification of Recombinant PiAP12

The domain of PiAP12 containing a C-terminal 6× His tag was obtained from *Escherichia coli* [BL21(DE3)T1r]. Briefly, cells were incubated in 2xYT at 37°C to OD_{600} = 0.8, and protein expression was induced with 1 mM IPTG for 6 h at 30°C. Cells were collected and lysed by sonication and the supernatant after ultracentrifugation applied to Fractogel EMD TMAE (M) resin (equilibrated with 20 mM Tris-HCl, pH 6.6). The elution fraction (20 mM Tris-HCl and 500 mM NaCl, pH 6.6) containing PiAP12 was diluted with His equilibration buffer (50 mM NaH_2PO_4, 300 mM NaCl, and 10 mM imidazole, pH 8.0) and applied to an equilibrated Ni-NTA column. After a washing step, the protein was eluted with 300 mM imidazole. The buffer of the elution fractions with PiAP12 was changed to 50 mM Tris-HCl, pH 8.0. In addition, impurities in the elution fraction of the supernatant were removed using denaturing conditions. For this, PiAP12 was diluted in urea buffer (50 mM NaH_2PO_4, 300 mM NaCl, 10 mM imidazole, and 8 M urea, pH 8.0), applied to Ni-NTA beads, and incubated for 1 h at room temperature under rotation. After a washing step, PiAP12 was eluted with 500 mM imidazole. Refolding was performed by a gradual buffer exchange over 60 h to 20 mM HEPES, 100 mM NaCl, and 0.2 mM DTT (pH 7.2), which resulted in semistable protein (Hodder et al., 2015).

In Vitro Cleavage Assays with AVR3a

Purified PiAP12 (180 μg) was incubated with 5 μg recombinant $AVR3a_{22\text{-}147}$ 6xHis containing the N-terminal RxLR motif for 1 h at 37°C. The reaction was stopped with SDS sample buffer and subsequent heating up to 90°C for 10 min. Samples were analyzed by SDS-PAGE and immunoblotting (anti-His antibody, 1:10,000; Qiagen; no. 34460).

For another assay, domains of all aspartic proteases from *P. infestans* were cloned (Kay et al., 2011). AVR3a and each domain were co-transformed into BL21(DE3)T1r. Cells containing both constructs were incubated in LB medium at 37°C to OD_{600} = 0.8, and protein expression was induced with 1 mM IPTG for 6 h at 30°C. Cells were collected (15 min, 4500*g*, 4°C) and lysed by sonication. The supernatant after a centrifugation step (30 min, 16,100*g*, 4°C) was analyzed by immunoblot with an α-5xHis antibody (1:10,000; Qiagen; no. 34460).

NMR Spectroscopy and Resonance Assignment

The 2D and 3D spectra were recorded at 25°C on a 700-MHz Ultrashield NMR spectrometer (Bruker) equipped with a triple cryoprobe head (Bruker Biospin). The 3D and 4D spectra were recorded with a Varian VNMRS 700 NMR spectrometer equipped with four RF channels, a Performa-XYZ PFG gradient unit, and a room temperature ^{1}H/^{13}C/^{15}N triple-resonance probe head. $AVR3a_{60\text{-}147}$ (300 μM in 50 mM KP_i buffer, pH 6.5) was prepared with 10% D_2O and 50 μM DSS as calibration standard. All spectra were analyzed with Sparky 3.113. For assignment, all 4D nonuniform sampled (NUS) NMR data sets were used. The process of sequentially specific assignment employing 4D NUS NMR data sets was performed with a 3D HNCO experiment based on NUS (1000 data points, maximal evolution times: 30 ms for ^{13}CO and 28 ms for ^{15}N, acquisition time: 6 h), a 4D HNCOCA NMR spectrum (Zawadzka-Kazimierczuk et al., 2010) correlating interresidual HN(i)-N(i)-CO(i-1)-Cα(i-1) resonances (1400 data points, maximum evolution times of 30 ms for ^{13}CO, 10 ms for ^{13}Cα, and 28 ms for ^{15}N, acquisition time: 18 h), the complementary 4D HNCACO (Zawadzka-Kazimierczuk et al., 2010), correlating both intraresidual HN(i)-N(i)-Cα(i)-CO(i) and interresidual HN(i)-N(i)-Cα(i-1)-CO(i-1) resonances (2500 data points, maximum evolution times of 20 ms for ^{13}CO, 10 ms for ^{13}Cα, and 28 ms for ^{15}N, acquisition time: 31 h), a 4D HBHACBCANH spectrum correlating ^{1}H, ^{13}C, and ^{15}N signals for intraresidual [HN(i)-N(i)-Cαβ(i)-Hαβ(i)] and interresidual [HN(i)-N(i)-Cαβ(i-1)-Hαβ(i-1)] resonances (2500 data points, maximum evolution times of 10 ms for ^{13}C, 7 ms for ^{1}H, and 28 ms for ^{15}N, acquisition time: 50 h). Additionally, aliphatic side chain ^{1}H and ^{13}C chemical shifts were assigned with HCCH-COSY, HCCH-TOCSY, HBHAHN, and HBHA(CO)NH spectra and aromatic side chain resonances were assigned from two-dimensional COSY, TOCSY, and NOESY spectra. Distance constraints were obtained from two ^{1}H-homonuclear NOESY spectra, one recorded in water, the other recorded in D_2O buffer, from the ^{13}C-NOESY-HSQC and the ^{15}N-NOESY-HSQC. The 3D ^{13}C-edited NOESY-HSQC spectra were acquired with a mixing time of 150 ms for aliphatic and aromatic regions on Varian VNMRS 800 NMR spectrometer equipped with four RF channels, a Performa IV PFG module, and cryogenic ^{1}H/^{13}C/^{15}N triple resonance probe head. Processing and evaluation of spectra were performed with Topspin 3.0 (Bruker) or NMRPipe (Delaglio et al., 1995); assignment was done with Sparky.

Structure Calculation

^{15}N and ^{13}C resonances were calibrated unidirectionally following the IUPAC-IUB recommended chemical shift referencing ratios (Wishart et al., 1995; Markley et al., 1998). NOE restraints were identified and transformed into distance constraints using the automated standard protocol of Cyana (Güntert et al., 1991). Dihedral angles were calculated using Talos$^+$ (Shen et al., 2009). The structure of $AVR3a_{60\text{-}147}$ was calculated using Cyana 2.1 (López-Méndez and Güntert, 2006) without using a homolog as a guide

structure. Energy minimization was performed with YASARA 11.12.31 (Krieger and Vriend, 2002).

Molecular Weight Estimation by Measuring Relaxation Constants

For estimation of the molecular weight of the AVR3a protein constructs, different spectra with varying relaxation times τ were recorded (20, 100, 150, 200, 300, 500, 750, 1000, and 1400 ms for T_1 and 10, 30, 50, 90, 130, 170, 210, and 250 ms for T_2). With the different signal intensities, the time constants T_1 and T_2 were calculated for each amino acid as described by Kay et al. (1992). For analysis, only resonances from amino acids located in secondary structure elements without contribution of chemical exchange processes were chosen (Blackledge et al., 1998). Subsequently, the rotation correlation time τ_c and the standard curve for the estimation of the molecular weight were calculated as described elsewhere (Rossi et al., 2010).

SEC

SEC experiments for $AVR3a_{48\text{-}147}$ wild type and the poly-E/Q mutant were performed in 50 mM NaP_i, 500 mM NaCl, pH 7.0, with Superdex 75 10/300 on a Bio-Rad system at a flow rate of 0.5 mL/min. The column was calibrated under the same conditions with thyroglobulin (670 kD), γ-globuline (158 kD), ovalbumin (44 kD), myoglobulin (17 kD), and vitamin B_{12} (1.35 kD); R^2 was 0.9199 after linear regression of the calibration standards.

Accession Numbers

Sequence data from this article can be found in the Arabidopsis Genome Initiative or GenBank/EMBL databases under the following accession numbers: AVR3a ($AVR3a^{EM}$, ADC96691.1; $AVR3a^{KI}$, ADC96694.1), PiAP01 (HM588685, corrected; Kay et al., 2011), PiAP02 (XP_002900284.1), PiAP04 (XP_002998816.1), PiAP05 (XP_002902303.1), PiAP06 (XP_002905662.1), PiAP07 (XP_002905687.1), PiAP08 (HM588686, corrected; Kay et al., 2011), PiAP09 (XP_002904877), PiAP10 (XP_002907533), PiAP11 (XP_002907534), and PiAP12 (XP_002901082). Structural coordinates and NMR shift data were deposited in the RCSB databank (entry ID: 2NAR) and in the BMRB databank (entry ID: rcsb104633), respectively. Structures already published, but used in this study are as follows: AVR3a4 (PDB-ID: 2LC2) and AVR3a11 (PDB-ID: 3ZGK).

Supplemental Data

Supplemental Table 1. Primers and restriction sites used for cloning of the constructs used in this study.

ACKNOWLEDGMENTS

Our work is supported by the BBSRC (S.W., C.J.S., and P.v.W.), NERC (P.v.W.), and the University of Aberdeen (C.J.S., P.v.W., and I.D.). This work was supported by EU East-NMR FP7 Project (Contract 228461) and Polish National Centre for Research and Development under research grant number 178479 (contract number PBS1/A9/13/2012) (for I.Z.). We thank Kevin MacKenzie of the core microscopy facility of the University of Aberdeen for helpful suggestions and Regine Kahmann for critical reading of the manuscript.

AUTHOR CONTRIBUTIONS

S.W., F.T., A.M., K.A., C.J.S., P.B., and P.v.W. designed research. S.W., F.T., A.M., K.A., U.L., I.Z., W.K., J.S., and I.D. performed research and analyzed data. S.W., F.T., C.J.S., and P.v.W. wrote the article. All authors have given approval to the final version of the manuscript.

Received July 8, 2016; revised April 4, 2017; accepted May 10, 2017; published May 18, 2017.

REFERENCES

Anderson, R.G., Casady, M.S., Fee, R.A., Vaughan, M.M., Deb, D., Fedkenheuer, K., Huffaker, A., Schmelz, E.A., Tyler, B.M., and McDowell, J.M. (2012). Homologous RXLR effectors from Hyaloperonospora arabidopsidis and *Phytophthora sojae* suppress immunity in distantly related plants. Plant J. **72:** 882–893.

Baker, N.A., Sept, D., Joseph, S., Holst, M.J., and McCammon, J.A. (2001). Electrostatics of nanosystems: application to microtubules and the ribosome. Proc. Natl. Acad. Sci. USA **98:** 10037–10041.

Bhattacharjee, S., Hiller, N.L., Liolios, K., Win, J., Kanneganti, T.D., Young, C., Kamoun, S., and Haldar, K. (2006). The malarial host-targeting signal is conserved in the Irish potato famine pathogen. PLoS Pathog. **2:** e50.

Blackledge, M., Cordier, F., Dosset, P., and Marion, D. (1998). Precision and uncertainty in the characterization of rotational diffusion from heteronuclear relaxation data. J. Am. Chem. Soc. **120:** 4538–4539.

Boddey, J.A., Moritz, R.L., Simpson, R.J., and Cowman, A.F. (2009). Role of the Plasmodium export element in trafficking parasite proteins to the infected erythrocyte. Traffic **10:** 285–299.

Boddey, J.A., Hodder, A.N., Günther, S., Gilson, P.R., Patsiouras, H., Kapp, E.A., Pearce, J.A., de Koning-Ward, T.F., Simpson, R.J., Crabb, B.S., and Cowman, A.F. (2010). An aspartyl protease directs malaria effector proteins to the host cell. Nature **463:** 627–631.

Boddey, J.A., et al. (2016). Export of malaria proteins requires co-translational processing of the PEXEL motif independent of phosphatidylinositol-3-phosphate binding. Nat. Commun. **7:** 10470.

Bos, J.I., et al. (2010). *Phytophthora infestans* effector AVR3a is essential for virulence and manipulates plant immunity by stabilizing host E3 ligase CMPG1. Proc. Natl. Acad. Sci. USA **107:** 9909–9914.

Bos, J.I., Kanneganti, T.D., Young, C., Cakir, C., Huitema, E., Win, J., Armstrong, M.R., Birch, P.R., and Kamoun, S. (2006). The C-terminal half of Phytophthora infestans RXLR effector AVR3a is sufficient to trigger R3a-mediated hypersensitivity and suppress INF1-induced cell death in *Nicotiana benthamiana*. Plant J. **48:** 165–176.

Chang, H.H., Falick, A.M., Carlton, P.M., Sedat, J.W., DeRisi, J.L., and Marletta, M.A. (2008). N-terminal processing of proteins exported by malaria parasites. Mol. Biochem. Parasitol. **160:** 107–115.

Chou, S., Krasileva, K.V., Holton, J.M., Steinbrenner, A.D., Alber, T., and Staskawicz, B.J. (2011). *Hyaloperonospora arabidopsidis* ATR1 effector is a repeat protein with distributed recognition surfaces. Proc. Natl. Acad. Sci. USA **108:** 13323–13328.

Coffey, M.J., et al. (2015). An aspartyl protease defines a novel pathway for export of Toxoplasma proteins into the host cell. eLife **4:** e10809.

Curt-Varesano, A., Braun, L., Ranquet, C., Hakimi, M.A., and Bougdour, A. (2016). The aspartyl protease TgASP5 mediates the export of the Toxoplasma GRA16 and GRA24 effectors into host cells. Cell. Microbiol. **18:** 151–167.

Delaglio, F., Grzesiek, S., Vuister, G.W., Zhu, G., Pfeifer, J., and Bax, A. (1995). NMRPipe: a multidimensional spectral processing system based on UNIX pipes. J. Biomol. NMR **6:** 277–293.

Dou, D., Kale, S.D., Wang, X., Jiang, R.H., Bruce, N.A., Arredondo, F.D., Zhang, X., and Tyler, B.M. (2008). RXLR-mediated entry of Phytophthora sojae effector Avr1b into soybean cells does not require pathogen-encoded machinery. Plant Cell **20:** 1930–1947.

Edman, P.H. (1950). Method for determination of the amino acid sequence in peptides. Acta Chem. Scand. **4:** 283–293.

Ellis, J.G., and Dodds, P.N. (2011). Showdown at the RXLR motif: Serious differences of opinion in how effector proteins from filamentous eukaryotic pathogens enter plant cells. Proc. Natl. Acad. Sci. USA **108:** 14381–14382.

Gan, P.H., Rafiqi, M., Ellis, J.G., Jones, D.A., Hardham, A.R., and Dodds, P.N. (2010). Lipid binding activities of flax rust AvrM and AvrL567 effectors. Plant Signal. Behav. **5:** 1272–1275.

Gilroy, E.M., Taylor, R.M., Hein, I., Boevink, P., Sadanandom, A., and Birch, P.R. (2011). CMPG1-dependent cell death follows perception of diverse pathogen elicitors at the host plasma membrane and is suppressed by Phytophthora infestans RXLR effector AVR3a. New Phytol. **190:** 653–666.

Grouffaud, S., van West, P., Avrova, A.O., Birch, P.R., and Whisson, S.C. (2008). *Plasmodium falciparum* and *Hyaloperonospora parasitica* effector translocation motifs are functional in *Phytophthora infestans*. Microbiology **154:** 3743–3751.

Gu, B., Kale, S.D., Wang, Q., Wang, D., Pan, Q., Cao, H., Meng, Y., Kang, Z., Tyler, B.M., and Shan, W. (2011). Rust secreted protein Ps87 is conserved in diverse fungal pathogens and contains a RXLR-like motif sufficient for translocation into plant cells. PLoS One **6:** e27217.

Güntert, P., Braun, W., and Wüthrich, K. (1991). Efficient computation of three-dimensional protein structures in solution from nuclear magnetic resonance data using the program DIANA and the supporting programs CALIBA, HABAS and GLOMSA. J. Mol. Biol. **217:** 517–530.

Hammoudi, P.M., et al. (2015). Fundamental roles of the Golgi-associated Toxoplasma aspartyl protease, ASP5, at the host-parasite interface. PLoS Pathog. **11:** e1005211.

Hiller, N.L., Bhattacharjee, S., van Ooij, C., Liolios, K., Harrison, T., Lopez-Estraño, C., and Haldar, K. (2004). A host-targeting signal in virulence proteins reveals a secretome in malarial infection. Science **306:** 1934–1937.

Hodder, A.N., et al. (2015). Structural basis for plasmepsin V inhibition that blocks export of malaria proteins to human erythrocytes. Nat. Struct. Mol. Biol. **22:** 590–596.

King, S.R., McLellan, H., Boevink, P.C., Armstrong, M.R., Bukharova, T., Sukarta, O., Win, J., Kamoun, S., Birch, P.R., and Banfield, M.J. (2014). *Phytophthora infestans* RXLR effector PexRD2 interacts with host MAPKKK ε to suppress plant immune signaling. Plant Cell **26:** 1345–1359.

Kale, S.D., et al. (2010). External lipid PI3P mediates entry of eukaryotic pathogen effectors into plant and animal host cells. Cell **142:** 284–295.

Kale, S.D., and Tyler, B.M. (2011). Entry of oomycete and fungal effectors into plant and animal host cells. Cell. Microbiol. **13:** 1839–1848.

Kay, J., Meijer, H.J., ten Have, A., and van Kan, J.A. (2011). The aspartic proteinase family of three Phytophthora species. BMC Genomics **12:** 254.

Kay, L.E., Nicholson, L.K., Delaglio, F., Bax, A., and Torchia, D.A. (1992). Pulse sequences for removal of the effects of cross-correlation between dipolar and chemical-shift anisotropy relaxation mechanism on the measurement of heteronuclear T1 and T2 values in proteins. J. Magn. Reson. **97:** 359–375.

Kemen, E., Gardiner, A., Schultz-Larsen, T., Kemen, A.C., Balmuth, A.L., Robert-Seilaniantz, A., Bailey, K., Holub, E., Studholme, D.J., Maclean, D., and Jones, J.D. (2011). Gene gain and loss during evolution of obligate parasitism in the white rust pathogen of *Arabidopsis thaliana*. PLoS Biol. **9:** e1001094.

Krieger, E., and Vriend, G. (2002). Models@Home: distributed computing in bioinformatics using a screensaver based approach. Bioinformatics **18:** 315–318.

Lokossou, A.A., Rietman, H., Wang, M., Krenek, P., van der Schoot, H., Henken, B., Hoekstra, R., Vleeshouwers, V.G., van der Vossen, E.A., Visser, R.G., Jacobsen, E., and Vosman, B. (2010). Diversity, distribution, and evolution of *Solanum bulbocastanum* late blight resistance genes. Mol. Plant Microbe Interact. **23:** 1206–1216.

López-Méndez, B., and Güntert, P. (2006). Automated protein structure determination from NMR spectra. J. Am. Chem. Soc. **128:** 13112–13122.

Lu, S., Chen, L., Tao, K., Sun, N., Wu, Y., Lu, X., Wang, Y., and Dou, D. (2013). Intracellular and extracellular phosphatidylinositol 3-phosphate produced by Phytophthora species is important for infection. Mol. Plant **6:** 1592–1604.

Lu, Y.J., Schornack, S., Spallek, T., Geldner, N., Chory, J., Schellmann, S., Schumacher, K., Kamoun, S., and Robatzek, S. (2012). Patterns of plant subcellular responses to successful oomycete infections reveal differences in host cell reprogramming and endocytic trafficking. Cell. Microbiol. **14:** 682–697.

Markley, J.L., Bax, A., Arata, Y., Hilbers, C.W., Kaptein, R., Sykes, B.D., Wright, P.E., and Wüthrich, K. (1998). Recommendations for the presentation of NMR structures of proteins and nucleic acids. Pure Appl. Chem. **70:** 117–142.

Marti, M., Good, R.T., Rug, M., Knuepfer, E., and Cowman, A.F. (2004). Targeting malaria virulence and remodeling proteins to the host erythrocyte. Science **306:** 1930–1933.

Marti, M., and Spielmann, T. (2013). Protein export in malaria parasites: many membranes to cross. Curr. Opin. Microbiol. **16:** 445–451.

Mirgorodskaya, E.N., Krogh, T., and Roepstorff, P. (2000). Characterization of protein glycosylation by MALDI-TOFMS. In Mass Spectrometry of Proteins and Peptides, J. Chapman, ed (Totowa, NJ: Humana Press), pp. 273–292.

Na, R., Yu, D., Qutob, D., Zhao, J., and Gijzen, M. (2013). Deletion of the *Phytophthora sojae* avirulence gene Avr1d causes gain of virulence on Rps1d. Mol. Plant Microbe Interact. **26:** 969–976.

Petre, B., and Kamoun, S. (2014). How do filamentous pathogens deliver effector proteins into plant cells? PLoS Biol. **12:** e1001801.

Petre, B., Kopischke, M., Evrard, A., Robatzek, S., and Kamoun, S. (2016). Cell re-entry assays do not support models of pathogen-independent translocation of AvrM and AVR3a effectors into plant cells. bioRxiv doi/10.1101/038232.

Plett, J.M., Kemppainen, M., Kale, S.D., Kohler, A., Legué, V., Brun, A., Tyler, B.M., Pardo, A.G., and Martin, F. (2011). A secreted effector protein of *Laccaria bicolor* is required for symbiosis development. Curr. Biol. **21:** 1197–1203.

Rafiqi, M., Gan, P.H., Ravensdale, M., Lawrence, G.J., Ellis, J.G., Jones, D.A., Hardham, A.R., and Dodds, P.N. (2010). Internalization of flax rust avirulence proteins into flax and tobacco cells can occur in the absence of the pathogen. Plant Cell **22:** 2017–2032.

Rossi, P., Swapna, G.V., Huang, Y.J., Aramini, J.M., Anklin, C., Conover, K., Hamilton, K., Xiao, R., Acton, T.B., Ertekin, A., Everett, J.K., and Montelione, G.T. (2010). A microscale protein NMR sample screening pipeline. J. Biomol. NMR **46:** 11–22.

Russo, I., Babbitt, S., Muralidharan, V., Butler, T., Oksman, A., and Goldberg, D.E. (2010). Plasmepsin V licenses Plasmodium proteins for export into the host erythrocyte. Nature **463:** 632–636.

Saunders, D.G., Breen, S., Win, J., Schornack, S., Hein, I., Bozkurt, T.O., Champouret, N., Vleeshouwers, V.G., Birch, P.R., Gilroy, E.M., and Kamoun, S. (2012). Host protein BSL1 associates with *Phytophthora infestans* RXLR effector AVR2 and the Solanum demissum Immune receptor R2 to mediate disease resistance. Plant Cell **24:** 3420–3434.

Shen, Y., Delaglio, F., Cornilescu, G., and Bax, A. (2009). TALOS+: a hybrid method for predicting protein backbone torsion angles from NMR chemical shifts. J. Biomol. NMR **44:** 213–223.

Starheim, K.K., Gevaert, K., and Arnesen, T. (2012). Protein N-terminal acetyltransferases: when the start matters. Trends Biochem. Sci. **37:** 152–161.

Stassen, J.H., den Boer, E., Vergeer, P.W., Andel, A., Ellendorff, U., Pelgrom, K., Pel, M., Schut, J., Zonneveld, O., Jeuken, M.J., and Van den Ackerveken, G. (2013). Specific in planta recognition of two GKLR proteins of the downy mildew *Bremia lactucae* revealed in a large effector screen in lettuce. Mol. Plant Microbe Interact. **26:** 1259–1270.

Sun, F., Kale, S.D., Azurmendi, H.F., Li, D., Tyler, B.M., and Capelluto, D.G. (2013). Structural basis for interactions of the *Phytophthora sojae* RxLR effector Avh5 with phosphatidylinositol 3-phosphate and for host cell entry. Mol. Plant Microbe Interact. **26:** 330–344.

Torto, T.A., Li, S., Styer, A., Huitema, E., Testa, A., Gow, N.A., van West, P., and Kamoun, S. (2003). EST mining and functional expression assays identify extracellular effector proteins from the plant pathogen Phytophthora. Genome Res. **13:** 1675–1685.

van Poppel, P.M., Guo, J., van de Vondervoort, P.J., Jung, M.W., Birch, P.R., Whisson, S.C., and Govers, F. (2008). The *Phytophthora infestans* avirulence gene Avr4 encodes an RXLR-dEER effector. Mol. Plant Microbe Interact. **21:** 1460–1470.

Wawra, S., Belmonte, R., Löbach, L., Saraiva, M., Willems, A., and van West, P. (2012a). Secretion, delivery and function of oomycete effector proteins. Curr. Opin. Microbiol. **15:** 685–691.

Wawra, S., Agacan, M., Boddey, J.A., Davidson, I., Gachon, C.M., Zanda, M., Grouffaud, S., Whisson, S.C., Birch, P.R., Porter, A.J., and van West, P. (2012b). Avirulence protein 3a (AVR3a) from the potato pathogen *Phytophthora infestans* forms homodimers through its predicted translocation region and does not specifically bind phospholipids. J. Biol. Chem. **287:** 38101–38109.

Whisson, S.C., et al. (2007). A translocation signal for delivery of oomycete effector proteins into host plant cells. Nature **450:** 115–118.

Win, J., Krasileva, K.V., Kamoun, S., Shirasu, K., Staskawicz, B.J., and Banfield, M.J. (2012). Sequence divergent RXLR effectors share a structural fold conserved across plant pathogenic oomycete species. PLoS Pathog. **8:** e1002400.

Wishart, D.S., Bigam, C.G., Yao, J., Abildgaard, F., Dyson, H.J., Oldfield, E., Markley, J.L., and Sykes, B.D. (1995). 1H, 13C and 15N chemical shift referencing in biomolecular NMR. J. Biomol. NMR **6:** 135–140.

Yaeno, T., Li, H., Chaparro-Garcia, A., Schornack, S., Koshiba, S., Watanabe, S., Kigawa, T., Kamoun, S., and Shirasu, K. (2011). Phosphatidylinositol monophosphate-binding interface in the oomycete RXLR effector AVR3a is required for its stability in host cells to modulate plant immunity. Proc. Natl. Acad. Sci. USA **108:** 14682–14687.

Yaeno, T., and Shirasu, K. (2013). The RXLR motif of oomycete effectors is not a sufficient element for binding to phosphatidylinositol monophosphates. Plant Signal. Behav. **8:** e23865.

Yu, X., Tang, J., Wang, Q., Ye, W., Tao, K., Duan, S., Lu, C., Yang, X., Dong, S., Zheng, X., and Wang, Y. (2012). The RxLR effector Avh241 from *Phytophthora sojae* requires plasma membrane localization to induce plant cell death. New Phytol. **196:** 247–260.

Zawadzka-Kazimierczuk, A., Kazimierczuk, K., and Koźmiński, W. (2010). A set of 4D NMR experiments of enhanced resolution for easy resonance assignment in proteins. J. Magn. Reson. **202:** 109–116.